Role of C_xN_y-Triazine in Photocatalysis for Efficient Hydrogen Generation and Organic Pollutant Degradation Under Solar Light Irradiation

*Chinh-Chien Nguyen, Nhu-Nang Vu, Stéphane Chabot, Serge Kaliaguine, and Trong-On Do**

A critical drawback of existing materials, which restricts the photocatalytic efficiency, is the fast recombination of charge carriers. To address this challenge, loading reduction and oxidation co-catalysts on two opposite surfaces of a hollow semiconductor is a critical approach to improve the photocatalytic performance. These co-catalysts mainly act as oxidation and reduction active sites, while suppressing the charge recombination. Moreover, the development of a novel and efficient co-catalyst that boosts charge separation is a very important feature for the photocatalytic performance. Herein, we report the first synthesis of hollow Pt/TiO_2/C_xN_y-triazine nanocomposite using carbon colloidal spheres as a hard template, in which Pt and C_xN_y-triazine are located on the two opposite hollow surfaces. C_xN_y-based triazine species formed from cyanamide during calcination do not only stabilize the hollow structure and significantly enhance the surface area of Pt/TiO_2/C_xN_y-triazine, but also act as an efficient oxidation co-catalysts. This new type of nanocomposite exhibits one of the best TiO_2-based photocatalysts working under solar light irradiation to date. It is 125 and 62 times higher than that of Pt/TiO_2–P25 for hydrogen generation and methanol decomposition, respectively.

Solar energy is an attractive and sustainable solution for major global energy and environmental issues.[1,2] Semiconductor-based photocatalysts are promising candidates for implementing this strategy because the photogenerated electron-hole pairs in an excited state can be used to either produce solar fuels or decompose organic pollutants without the addition of strong oxidizing agents.[3] Over the past decades, many semiconductors have been identified as potential photocatalysts.[4] However, a critical drawback of the existing photocatalysts, which restricts the photocatalytic efficiency, is the fast recombination of charge carriers.[5] To address this challenge, hollow semiconductor nanocomposites possessing high surface area and two separate co-catalysts that drive the migration of the photogenerated electrons and holes to opposite directions have been developed. This design not only improves the charge separation, but also favors the surface catalytic reactions by reducing the activation energy.[6,7]

We have recently reported a hollow hybrid metal oxide-TiO_2 nanocomposite (e.g., Pt-TiO_2-Fe_xO_y) in which the reduction (Pt) and oxidation (Fe_xO_y) co-catalysts are located on two opposite surfaces of the structure. The separated co-catalysts and thin wall of this hollow nanocomposite improved the electron-hole separation, and as a result, enhanced the photocatalytic activity for H_2 generation.[8] Such nanocomposites afford the abundance of exposed active sites on the surface and reduce the diffusion length of the photogenerated charge carriers to the surface, thereby significantly enhancing charge separation.[9] In addition to the studies of reduction co-catalysts, discovering novel oxidation co-catalysts has been gaining increasing attention over the past few years.[10] The aim of a robust oxidation co-catalyst is to induce a significant change at the interface with semiconductor, which remarkably facilitates the charge transfer in a way that photogenerated holes are promoted to the surface active sites to oxidize the water molecules.[11] However, only a bit of information about such a study of co-catalysts is reported. Therefore, the development of a novel and efficient co-catalyst that boosts charge separation and shows a superior photocatalytic performance is a great challenge.

In this study, we discover a new type of hollow Pt/TiO_2/C_xN_y-triazine nanocomposite (denoted as Pt-TiO_2-C_xN_y) in which Pt and C_xN_y-triazine act as the reduction and oxidation co-catalysts. This type of nanocomposite is synthesized by using carbon colloidal spheres and cyanamide as the hard template and the precursor of C_xN_y-triazine species, respectively. The three-step synthesis of this nanocomposite is depicted in Scheme 1 (see Supporting Information [SI] for details). The calcination step is critical, as it not only generates pores within the hollow shells and high surface area by removing the carbon core and

T.-O. Do, C.-C. Nguyen, N.-N. Vu, S. Kaliaguine

Department of Chemical Engineering, Laval University, 1065, avenue de la Médecine, Québec, Canada G1V 0A6
E-mail: trong-on.do@gch.ulaval.ca

S. Chabot
EXP Inc., 5400 Boul. des Galeries, Bureau 205 Québec, QC, Canada G2K 2B4

DOI: 10.1002/solr.201700012

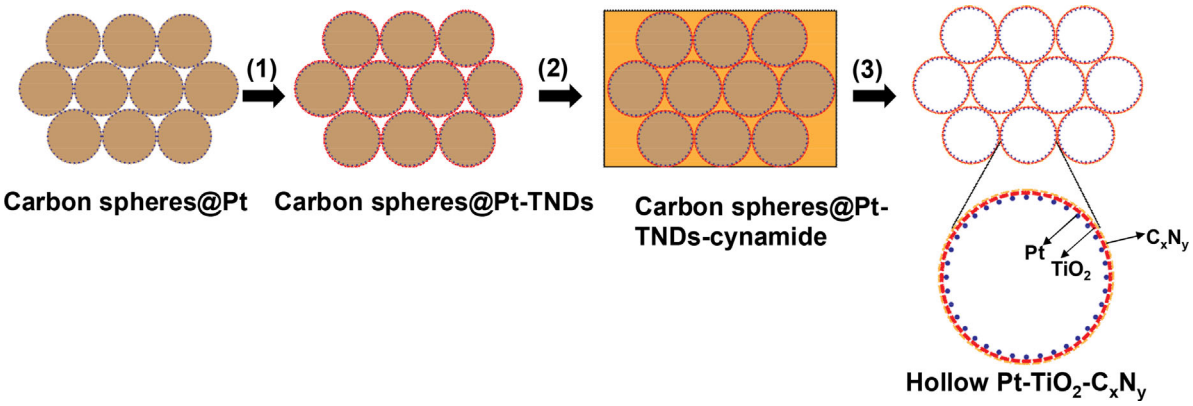

Scheme 1. Schematic illustration for the synthesis of Pt-TiO_2-C_xN_y: 1) one-pot synthesis of carbon@Pt, followed by coating titanate nanodisks (TNDs) using a layer-by-layer technique to obtain core-shell carbon spheres@Pt-TNDs, as previously described; 2) loading of cyanamide at 70 °C; and 3) calcination in air at 550 °C for 5 h to obtain Pt-TiO_2-C_xN_y.

polyethyleneimine, but also forms C_xN_y-triazine species, instead of the graphitic C_3N_4 (g-C_3N_4) obtained by using the conventional methods. The obtained nanocomposite shows a strong enhancement of photocatalytic activities for both hydrogen generation and methanol degradation under solar light irradiation, which originates from the critical contribution of C_xN_y-triazine species, functioning as stabilizers and oxidation co-catalyst. This new type of nanocomposite is one of the best TiO_2-based photocatalysts working under solar irradiation to date.

The X-ray diffraction (XRD) pattern of Pt-TiO_2-C_xN_y indicates the presence of TiO_2 and Pt (**Figure 1**A). The peak at $2\theta = 25.2°$ corresponds to the anatase phase of TiO_2 (110),[12,13] and the peaks centered at $2\theta = 39.8°$ and 46.3° are assigned to metallic Pt nanoparticles in the material.[14] Figure 1B shows the UV-Vis spectra of Pt-TiO_2-C_xN_y and Pt-TiO_2-550 prepared by using the same procedure, but without cyanamide. Pt-TiO_2-550 exhibits the main absorption band below 400 nm which is assigned to anatase TiO_2.[3,15] However, Pt-TiO_2-C_xN_y shows two intense absorption bands at ~260 and 350 nm; in addition, a weak and broadband at 400–650 nm was also observed. This is due to the presence of C_xN_y species in Pt-TiO_2-C_xN_y nanocomposite. Moreover, as seen in the inset of Figure 1B, for Pt-TiO_2-C_xN_y, in the range of <400 nm, one band gap energy at 3.2 eV is from TiO_2, and the second one at 3.4 eV is assigned to the band energy of the C_xN_y species in Pt-TiO_2-C_xN_y.

The Fourier transform infrared (FT-IR) spectrum of Pt-TiO_2-C_xN_y (line a, Figure S2A) reveals multiple IR bands in the region of 1300–1700 cm^{-1}, which are attributed to C–N heterocyclic stretches in the triazine units, while the band at ~3150 cm^{-1} is assigned to N–H stretching.[16] Therefore, cyanamide loaded on the outer surface of the carbon colloidal spheres induced the formation of heterocyclic structures instead of graphitic g-C_3N_4, obtained by the conventional method from the same precursor (line b, Figure S2A). As shown in Figure S2B, the FR-IR spectrum of Pt-TiO_2-C_xN_y shows the bands in the region of 3300–3700 cm^{-1}, which could be assigned to O–H stretching of hydroxyl groups on TiO_2 surface, whereas these are absent in g-C_3N_4 and Pt-TiO_2-550, respectively.[17] This indicates the remarkably high amount of hydroxyl groups on the TiO_2 surface in Pt-TiO_2-C_xN_y.

The chemical states of the elements in Pt-TiO_2-C_xN_y were investigated using X-ray photoelectron spectroscopy (XPS). The presence of Pt, Ti, O, N, and C was confirmed by the survey spectrum (Figure S3). The amount of C_xN_y and Pt were determined to be 0.8 and 2.1%, respectively by XPS. As seen in Figure S4, the peaks at 458.59 and 464.30 eV in the XPS spectrum of Ti2p are characteristic of Ti^{4+} in TiO_2 anatase.[18] For the Pt4f XPS spectrum (Figure S5), the peaks located at 71.16 and 74.49 eV are assigned to metallic Pt on TiO_2.[19] The C1s and N1s XPS spectra were also analyzed to indicate the nature of C_xN_y species. As shown in Figure 1C, the deconvolution of the C1s spectrum reveals three peaks: the peaks at 285.0 and 286.5 eV are attributed to adventitious carbon and C—N bonds, respectively; whereas, the peak at 289.0 eV corresponds to N = C–N in N-containing aromatic rings.[20] The deconvoluted N1s spectrum in Figure 1D exhibits the main peak at 398.2 eV assigned to sp^2-hybridized aromatic N_2 bonded to carbon atoms (C=N–C) in triazine. The peak at 400.35 eV is assigned to tertiary N_1 bonded to carbon atoms (N–$(C)_3$ or H–N–$(C)_2$), while the peak centered at 405.18 eV is attributed to π-excitation, as depicted in Figure S6.[21] Moreover, a small peak at 395.80 eV, which is assigned to Ti-N bond in TiO_2 lattice, was also observed.[22] The interaction of C_xN_y and TiO_2 was examined by comparing the O1s XPS spectra of Pt-TiO_2-C_xN_y and Pt-TiO_2-550 (Figure 1E). The main peak centered at 529.97 eV is assigned to O in the TiO_2 lattice, whereas, the other one is attributed to hydroxyl groups on the surface. Notably, the hydroxyl group content in Pt-TiO_2-C_xN_y is much higher than that in Pt-TiO_2-550, which is consistent with the FT-IR results, indicating that the former can trap more photogenerated holes, thus hindering the electron-hole recombination.[23,24] Importantly, a significant shift was observed in the binding energies of the hydroxyl group peak, which is induced by the presence of C_xN_y on the TiO_2 surface. This shift toward lower binding energies for Pt-TiO_2-C_xN_y indicates a higher electron density on the surface of O atoms derived from the strong interfacial interaction between the C_xN_y species and TiO_2, which should enhance the migration of the photogenerated holes and help separate charge carriers.[25] The above analyses afford two important findings: i) this synthesis could produce C_xN_y-based triazine species rather than

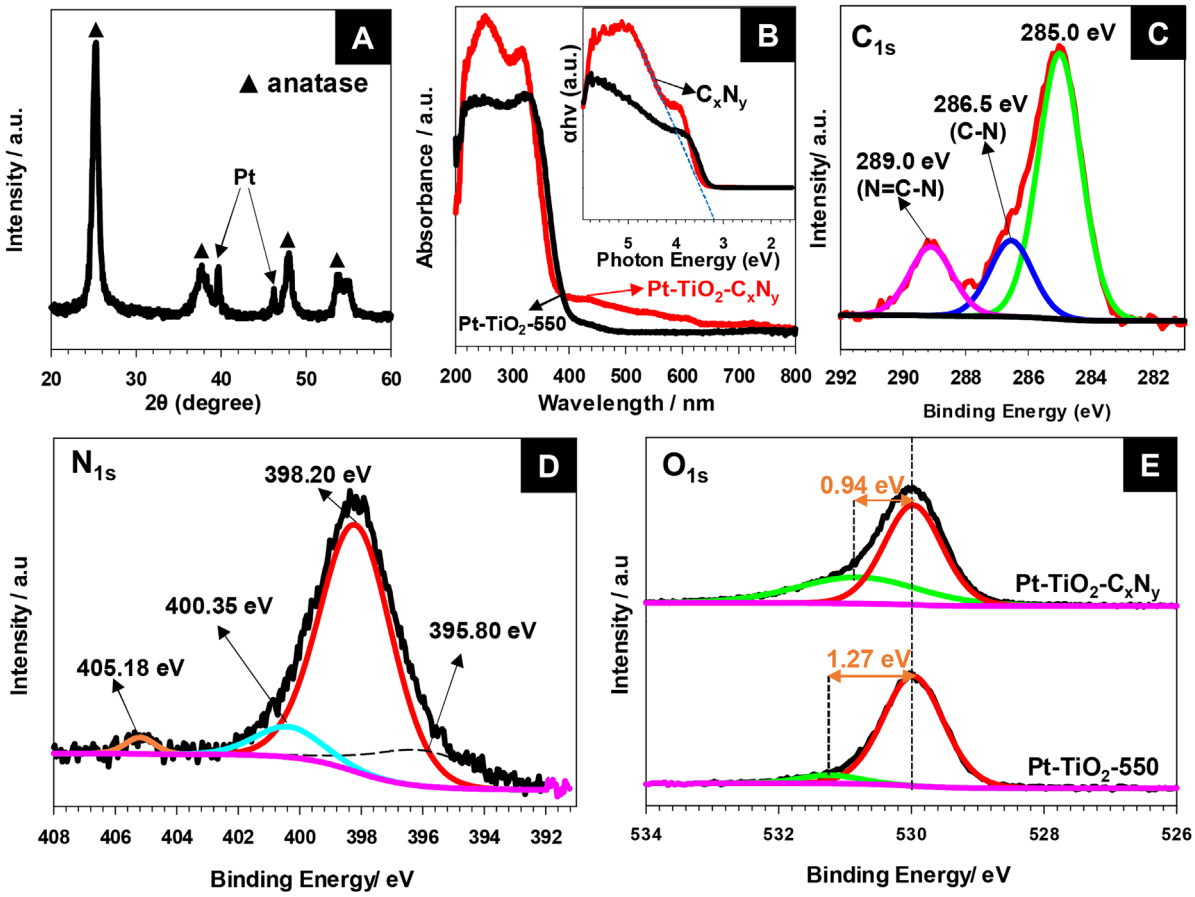

Figure 1. A) Powder XRD spectrum of Pt-TiO_2-C_xN_y and B) UV-Vis spectra of Pt-TiO_2-C_xN_y (red) and Pt-TiO_2-550 (black). Inset: plot of ($\alpha h\nu$) versus photon energy to determine band gap energies. C, D) C1s and N1s XPS spectrum of Pt-TiO_2-C_xN_y. E) O1s XPS spectra of Pt-TiO_2-C_xN_y and Pt-TiO_2-550.

tri-*s*-triazine or graphite carbon nitride, both of which are formed under conventional conditions[26,27]; ii) the obtained C_xN_y species induced a strong interaction with TiO_2 and enhanced the interfacial electronic states. Consequently, the migration of the photogenerated holes could be facilitated, which leads to a significant improvement in the charge separation. C_xN_y-triazine species, could therefore, act as oxidation co-catalysts.

Figure 2 shows scanning electron microscopy (SEM) images of the carbon colloidal spheres@Pt/titanate nanodisks (TNDs) before (Figure 2A) and after calcination (Figure 2B), denoted as Pt-TiO_2-C_xN_y. In addition, the transmission electron microscopy (TEM) image of Pt-TiO_2-C_xN_y is also shown in Figure S7. As seen in Figure 2A, after loading TNDs, the nanospheres are quite uniform in size and shape. However, subsequently, after loading cyanamide followed by calcination, this material changed its morphology into the hollow Pt-TiO_2-C_xN_y structure (Figure 2B). TEM image of a broken Pt-TiO_2-C_xN_y sphere in Figure 2C shows the presence of Pt nanoparticles inside the hollow structure (indicated by red dashed circles). The high-resolution TEM image (Figure 2D) and the corresponding energy-dispersive X-ray spectroscopy (EDS) results (Figure S8) show the lattice spacing (0.352 nm) corresponding to d(101) of TiO_2 anatase and a Pt nanoparticle size of ~12 nm.[28] Figure 2D also shows the intimate contact between Pt and TiO_2. This close contact between metal and semiconductor may enhance the charge transfer between them, and thus, the photocatalytic efficiency. **Figure 3** shows the STEM image and corresponding EDS elemental mapping over the selected area of Pt-TiO_2-C_xN_y indicating the homogeneous distribution of Pt, C, O, N, and Ti. The C signal is relatively weak due to the small amount of C_xN_y in the sample. Nitrogen could not be distinguished from Ti, because the amount of N is very low and the N peak is convoluted with Ti L alpha.

The photocatalytic activity of Pt-TiO_2-C_xN_y was carried out and compared with those of other photocatalysts including Pt-TiO_2-550, Pt-TiO_2 (P25), and Pt-bulk C_3N_4 for the hydrogen generation and for the decomposition of methanol to CO_2 under simulated solar irradiation (see SI for details). Pt-TiO_2-C_xN_y exhibits a much higher photocatalytic activity for the hydrogen generation than the other photocatalysts under the same photocatalytic conditions (**Figure 4**A). The generated amount of H_2 for Pt-TiO_2-C_xN_y is 125 and 10.7 times higher than those of Pt-TiO_2 (P25) and Pt-bulk C_3N_4, respectively. Importantly, the amount of hydrogen produced by Pt-TiO_2-C_xN_y is ~10 times higher than that of Pt-TiO_2-550 (without C_xN_y-triazine), which confirms the critical contribution of C_xN_y-triazine species to the photocatalytic activity. It is also noteworthy that it also presented the highest photocatalytic activity among the solar-driven TiO_2-based

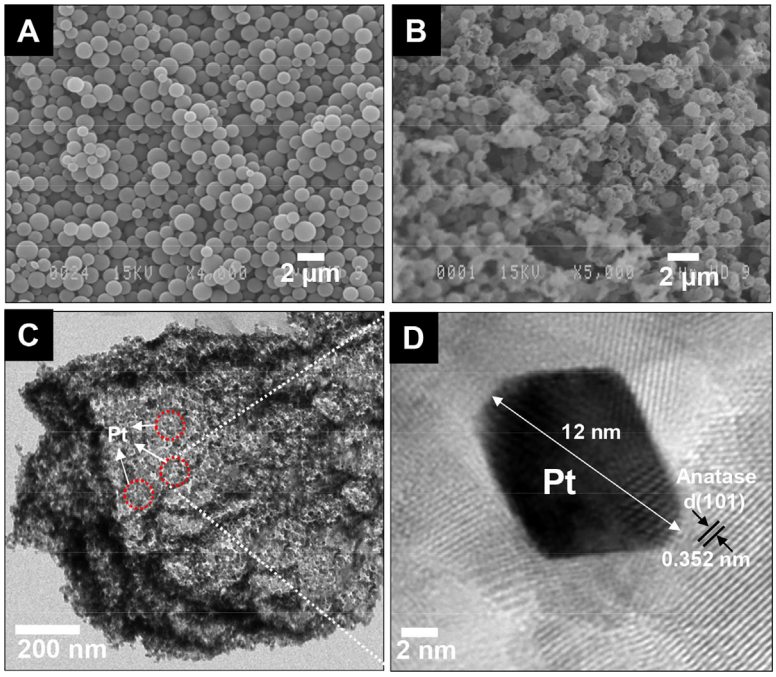

Figure 2. SEM images of A) carbon colloidal spheres@Pt/TND and B) Pt-TiO_2-C_xN_y; C) TEM, and D) high-resolution TEM images of the interior of the broken Pt-TiO_2-C_xN_y sphere, respectively.

photocatalysts (Table S1). Moreover, the improvement factor (IF) was introduced to represent the ability of the photocatalysts. It was measured by comparing the photoactivity of the prepared samples to TiO_2 (P25), which was considered as the reference photocatalyst, in the same test conditions. It can be seen that Pt-TiO_2-C_xN_y shows the highest improvement factor, as shown in Table S1. Therefore, this new type of nanocomposite exhibits one of the most efficient TiO_2-based photocatalysts working under solar light irradiation.

The photocatalytic efficiency (PE) of the material was calculated to be ~0.472% in the full solar spectrum (see calculations in SI). To the best of our knowledge, this is the highest PE value reported for TiO_2-based photocatalysts for hydrogen production to date. The photo-stability of Pt-TiO_2-C_xN_y was studied by multi-cycle photocatalytic experiments under the same conditions (Figure S10). No significant change in photoactivity was observed after three cycles (i.e., 15 h of reaction), indicating high stability for hydrogen production of this material. The photo-degradation of methanol on Pt-TiO_2-C_xN_y was also investigated under simulated solar irradiation (see SI). CO_2 as the final product of methanol oxidation, the amount of evolved CO_2 in

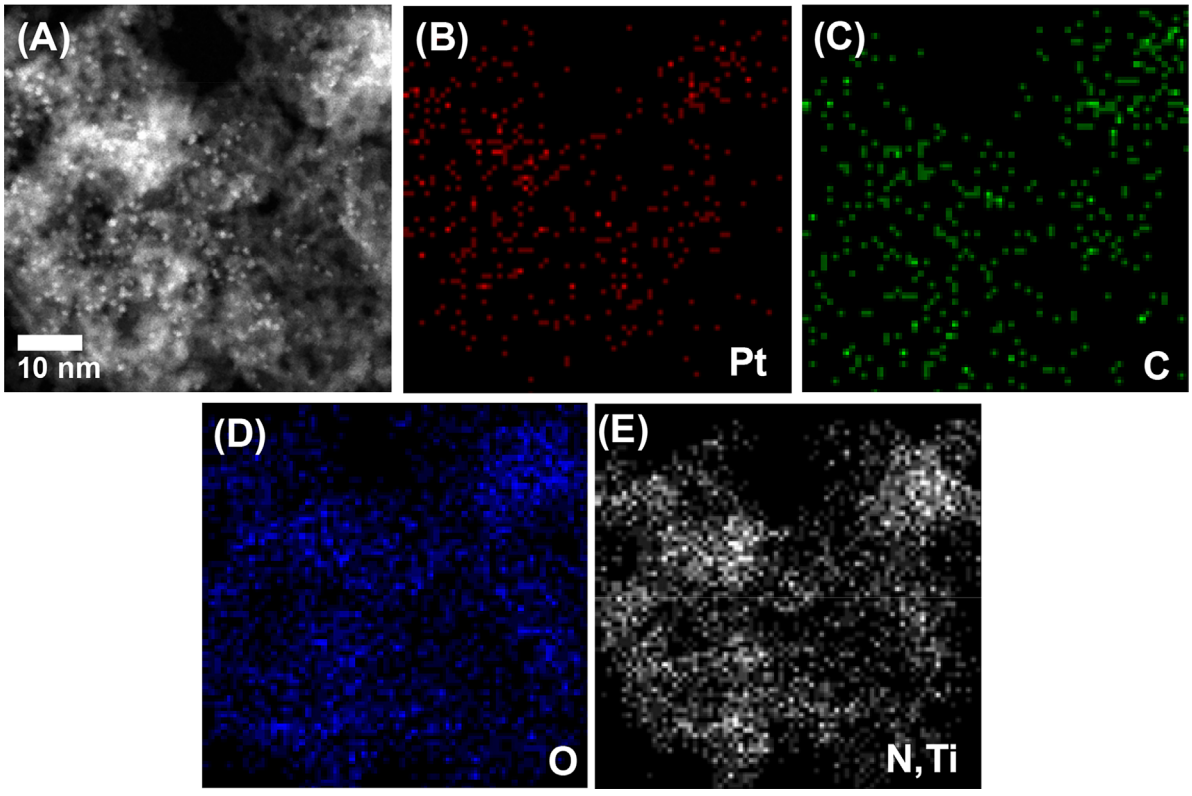

Figure 3. A) STEM image and EDS elemental mapping of B) platinum, C) carbon, D) oxygen, and E) nitrogen and titanium in the selected region of Pt-TiO_2-C_xN_y.

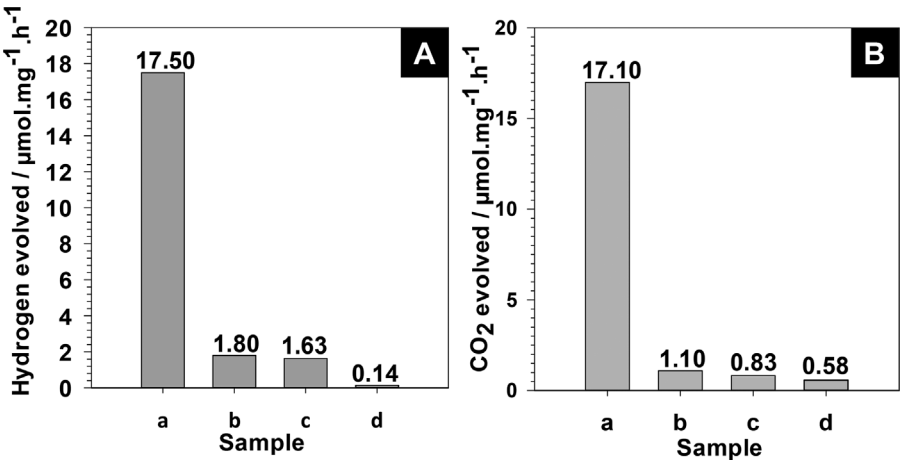

Figure 4. Production of (A) H_2 from water and (B) CO_2 from methanol degradation under simulated solar light (AM 1.5; 100 mW cm^{-2}) using a) Pt-TiO_2-C_xN_y, b) Pt-TiO_2-550, c) Pt-C_3N_4, and d) Pt-TiO_2 (P25) photocatalysts.

the presence of Pt-TiO_2-C_xN_y was considerably higher than that of other catalysts (Figure 4B). The corresponding PE value for Pt-TiO_2-C_xN_y under full solar light is ~1.38%, which is also among the highest values reported for the degradation of organic compounds. Thus, the obtained Pt-TiO_2-C_xN_y photocatalyst is promising for environmental remediation.

To understand this remarkable enhancement in photoactivity of this Pt-TiO_2-C_xN_y material, its texture and the role of C_xN_y-triazine species were also examined. The specific surface area is an important parameter because the photocatalytic activity strongly depends on the density of the active sites on the surface. The porous nature of Pt-TiO_2-C_xN_y was characterized using N_2 physical adsorption at 77 K. The N_2 isotherm of Pt-TiO_2-C_xN_y in Figure S11A exhibits an extremely high adsorption capacity at a high relative pressure ($P/P_0 = 0.85$–1), suggesting a largely porous structure.[29] Its specific surface area (e.g., 340 $m^2 \cdot g^{-1}$, Table S2) is the highest reported value for TiO_2 materials,[12,30] and ~7 times higher than that of commercial TiO_2-P25 (e.g. 50 $m^2 \cdot g^{-1}$). The pore size distribution in Figure S11B, calculated from the adsorption branch using the Barrett–Joyner–Halenda (BJH) method, stands in the range of 1–14 nm. The high specific surface area and large pore volume of Pt-TiO_2-C_xN_y could facilitate mass transfer and effectively accelerate the photocatalytic reaction.[31] The specific surface area of Pt-TiO_2-C_xN_y is twice than that of Pt-TiO_2-500 (170 $m^2 \cdot g^{-1}$) in the absence of C_xN_y indicating the role of C_xN_y-triazine species as a stabilizer to generate high surface area during calcination.

The role of C_xN_y- triazine species during photocatalysis was also studied by the photocatalytic overall water splitting (e.g., in the absence of sacrificial agent) for Pt-TiO_2-C_xN_y and other samples (Figure S12). The low specific surface area of the sample of Pt-TiO_2-C_xN_y (denoted as Pt-TiO_2-C_xN_y-L, 110 $m^2 \cdot g^{-1}$, Table S2) was prepared by using the same procedure as for the synthesis of Pt-TiO_2-C_xN_y, except that only one deposition of TNDs was done. The amount of hydrogen produced with Pt-TiO_2-C_xN_y was ~2 times and ~19 times higher than those of Pt-TiO_2-C_xN_y-L and Pt-TiO_2-550, respectively, while the amount of hydrogen produced with Pt-TiO_2 (P25) was negligible. The presence of C_xN_y in Pt-TiO_2-C_xN_y-L strongly enhances the photocatalytic activity even at its lower surface in comparison to that of Pt-TiO_2-550. This could be assigned to the important role of C_xN_y-triazine species for the charge separation. Additionally, the activity of Pt-TiO_2-C_xN_y is nearly double than that of Pt-TiO_2-C_xN_y-L, indicating that the high surface area significantly contributes to the improvement of the photocatalytic activity. Furthermore, photocatalytic activity for hydrogen generation in the absence of Pt as co-catalyst was also studied. Pt-free TiO_2-C_xN_y (denoted as TiO_2-C_xN_y), Pt-free TiO_2-C_xN_y-L (denoted as TiO_2-C_xN_y-L), and Pt-free TiO_2-550 (denoted as TiO_2-550) were prepared using the same procedures as for the synthesis of Pt-TiO_2-C_xN_y and Pt-TiO_2-C_xN_y-L, except that no Pt and Pt/C_xN_y, precursors were added, respectively. In the presence of the sacrificial agent, the amount of hydrogen generated with TiO_2-C_xN_y was ~310 µmol $\cdot g^{-1} \cdot h^{-1}$, which was 2.2 and 32 times higher than those generated with TiO_2-C_xN_y-L and TiO_2-550, respectively, while no evolved hydrogen was detected with commercial TiO_2-P25 (Figure S13). It can be concluded that the simultaneous presence of Pt nanoparticles (reduction co-catalyst) and C_xN_y-triazine species (oxidation co-catalyst) significantly boost the photocatalytic activities. Moreover, it should be noted that during the photodecomposition of methanol, for Pt-TiO_2-C_xN_y, the solution pH decreased (from neutral to acidic), while it slightly increased for both Pt-TiO_2-550 and Pt-TiO_2-P25. The decrease in pH is attributed to the oxidation reaction as follows: $H_2O + h^+ \rightarrow OH^\bullet + H^+$.[32] Therefore, C_xN_y-triazines on Pt-TiO_2 nanocomposite can attract photogenerated holes, thereby enhancing the charge separation and producing strongly oxidizing radicals ($OH^\bullet$); this process results in the production of H^+ from H_2O, which decreases the pH of the solution. Additionally, the separation of the photoinduced electron-hole pairs was also shown in Figure S14 by a photoluminescence (PL) spectra. The PL emission intensity of Pt-TiO_2-C_xN_y is significantly lower than that of Pt-TiO_2 (P25), Pt-TiO_2-550 and Pt-TiO_2-C_xN_y-L, indicating the remarkable improvement of charge separation for Pt-TiO_2-C_xN_y. Therefore, more carriers are available during the photocatalytic reactions. These findings, which are consistent with the results

obtained from characterization analyses and photocatalytic evaluation, provide the evidence for the role of C_xN_y triazine species as an oxidation co-catalyst, which attracts photogenerated holes leading to a remarkably enhanced charge separation.

Based on these findings, a possible mechanism for the enhanced photocatalytic activity of Pt-TiO_2-C_xN_y is proposed. As depicted in Figure S15, electrons from C_xN_y-triazines could transfer to the TiO_2 conduction band prior to being injected into Pt sites for the reduction reaction. Due to the presence of C_xN_y-triazine species on the surface of TiO_2, which function as oxidation co-catalysts, the migration of the photogenerated holes is facilitated by C_xN_y for the oxidation reaction of TEA (for hydrogen production) and water, to produce strong oxidation radicals (for the decomposition of methanol). This electron-hole separation, along with the very high specific surface area, results in the impressive reactivity of this photocatalyst.

In summary, we have prepared a new type of hollow Pt-TiO_2-C_xN_y nanocomposite using colloidal carbon spheres as a sacrificial template. The obtained photocatalyst shows an efficient catalytic activity for both hydrogen production and methanol oxidation under solar light irradiation. The enhanced photocatalytic activity is associated with the presence of C_xN_y-triazine species, as efficient co-catalysts, and the high specific surface area. This type of material is stable under photocatalytic conditions. We are currently trying to gain further insight into the detailed mechanisms of these processes (especially the structure and role of C_xN_y-triazine species), as well as developing materials with full solar spectrum absorption based on this strategy.

Supporting Information

Additional supporting information may be found in the online version of this article at the publisher's website.

Acknowledgments

This work was supported by the Natural Science and Engineering Research Council of Canada (NSERC) through the Collaborative Research and Development (CRD), Strategic Project (SP) and Discovery Grants. The author would like to thank EXP Inc. and SiliCycle Inc. for their support.

Final Version: March 27, 2017
Received: January 20, 2017
Revised: March 20, 2017

[1] Li, X., Yu, J., Jaroniec, M., *Chem. Soc. Rev.* **2016**, *45*, 2603.
[2] Chang, X., Wang, T., Gong, J., *Energy Environ. Sci.* **2016**, *9*, 2177.
[3] Nolan, M., Iwaszuk, A., Lucid, A. K., Carey, J. J., Fronzi, M., *Adv. Mater.* **2016**, *28*, 5425.
[4] a)Zhou, X., Häublein, V., Liu, N., Nguyen, N. T., Zolnhofer, E. M., Tsuchiya, H., Killian, M. S., Meyer, K., Frey, L., Schmuki, P., *Angew. Chem. Int. Ed.* **2016**, *55*, 3763. b)Park, H., Kim, H.-i., Moon, G.-h., Choi, W., *Energy Environ. Sci.* **2016**, *9*, 411.
[5] Cao, S., Yu, J.,*J. Photochem. Photobiol. C: Photochem. Rev.* **2016**, *27*, 72.
[6] a)Xie, S., Zhang, Q., Liu, G., Wang, Y., *Chem. Commun.* **2016**, *52*, 35. b)Jiao, Y., Jiang, H., Chen, F., *ACS Catal.* **2014**, *4*, 2249. c) Gholipour, M. R., Dinh, C.-T., Béland, F., Do, T.-O., *Nanoscale* **2015**, *7*, 8187.
[7] a)Marschall, R., *Adv. Funct. Mater.* **2014**, *24*, 2421. b)Li, A., Chang, X., Huang, Z., Li, C., Wei, Y., Zhang, L., Wang, T., Gong, J., *Angew. Chem. Int. Ed.* **2016**, *55*, 13734. c)Wang, D., Hisatomi, T., Takata, T., Pan, C., Katayama, M., Kubota, J., Domen, K., *Angew. Chem. Int. Ed.* **2013**, *52*, 11252.
[8] Pham, M.-H., Dinh, C.-T., Vuong, G.-T., Ta, N.-D., Do, T.-O., *Phys. Chem. Chem. Phys.* **2014**, *16*, 5937.
[9] a)Nguyen, C.-C., Vu, N.-N., Do, T.-O.,*J. Mater. Chem. A* **2016**, *4*, 4413. b)Cao, S., Low, J., Yu, J., Jaroniec, M., *Adv. Mater.* **2015**, *27*, 2150. c) Koutsouroubi, E. D., Xylouri, A. K., Armatas, G. S., *Chem. Commun.* **2015**, *51*, 4481. d)Meng, A., Zhang, J., Xu, D., Cheng, B., Yu, J., *Appl. Catal. B* **2016**, *198*, 286.
[10] a)Yang, J., Wang, D., Han, H., Li, C., *Acc. Chem. Res.* **2013**, *46*, 1900: b)Ran, J., Zhang, J., Yu, J., Jaroniec, M., Qiao, S. Z., *Chem. Soc. Rev.* **2014**, *43*, 7787. c)Gaikwad, A. P., Tyagi, D., Betty, C. A., Sasikala, R., *Appl. Catal. A* **2016**, *517*, 91. d)Wang, P., Lu, Y., Wang, X., Yu, H., *Appl. Surf. Sci.* **2017**, *391*, Part B 259.
[11] Yao, T., Chen, R., Li, J., Han, J., Qin, W., Wang, H., Shi, J., Fan, F., Li, C., *J. Am. Chem. Soc.* **2016**, *138*, 13664.
[12] Ismail, A. A., Bahnemann, D. W., *J. Mater. Chem.* **2011**, *21*, 11686.
[13] Serpone, N., Lawless, D., Khairutdinov, R., *J. Phys. Chem.* **1995**, *99*, 16646.
[14] Yu, J., Qi, L., Jaroniec, M., *J. Phys. Chem. C* **2010**, *114*, 13118.
[15] Cargnello, M., Montini, T., Smolin, S. Y., Priebe, J. B., Jaén, J. J. D., Doan-Nguyen, V. V., McKay, I. S., Schwalbe, J. A., Pohl, M.-M., Gordon, T. R., *Proc. Natl. Acad. Sci. USA* **2016**, *113*, 3966.
[16] Han, Q., Wang, B., Gao, J., Cheng, Z., Zhao, Y., Zhang, Z., Qu, L., *ACS Nano* **2016**, *10*, 2745.
[17] Erdem, B., Hunsicker, R. A., Simmons, G. W., Sudol, E. D., Dimonie, V. L., El-Aasser, M. S., *Langmuir* **2001**, *17*, 2664.
[18] Li, L., Yan, J., Wang, T., Zhao, Z.-J., Zhang, J., Gong, J., Guan, N., *Nat. Commun.* **2015**, *6*, 5881; Sinhamahapatra, A., Jeon, J.-P., Yu, J.-S., *Energy Environ. Sci.* **2015**, 8, 3539.
[19] Zhang, F., Chen, J., Zhang, X., Gao, W., Jin, R., Guan, N., Li, Y., *Langmuir* **2004**, *20*, 9329.
[20] a)Reddy, A. L. M., Srivastava, A., Gowda, S. R., Gullapalli, H., Dubey, M., Ajayan, P. M., *ACS Nano* **2010**, *4*, 6337. b)Zhang, Y., Cao, B., Zhang, B., Qi, X., Pan, C., *Thin Solid Films* **2012**, *520*, 6850. c)Huang, H., Yang, S., Vajtai, R., Wang, X., Ajayan, P. M., *Adv. Mater.* **2014**, *26*, 5160.
[21] a)Ong, W.-J., Tan, L.-L., Ng, Y. H., Yong, S.-T., Chai, S.-P., *Chem. Rev.* **2016**, *116*, 7159. b)Guo, Q., Xie, Y., Wang, X., Zhang, S., Hou, T., Lv, S., *Chem. Commun.* **2004**, *26*, 26–27. c)Thomas, A., Fischer, A., Goettmann, F., Antonietti, M., Muller, J.-O., Schlogl, R., Carlsson, J. M., *J. Mater. Chem.* **2008**, *18*, 4893.
[22] a)Sun, P., Lin, R., Wang, Z., Qiu, M., Chai, Z., Zhang, B., Meng, H., Tan, S., Zhao, C., Mai, W., *Nano Energy* **2017**, *31*, 432. b)Kim, C.-S., Shin, J.-W., Cho, Y.-H., Jang, H.-D., Byun, H.-S., Kim, T.-O., *Appl. Catal. A* **2013**, *455*, 211.
[23] Yu, J., Zhao, X., Zhao, Q., *Thin solid films* **2000**, *379*, 7; Eskandarloo, H. Badiei, A., Behnajady, M. A., Mohammadi Ziarani, G., *Photochem. Photobiol.* **2015**, 91, 797.
[24] McCafferty, E., Wightman, J., *Surf. Interface Anal.* **1998**, *26*, 549.
[25] a)Li, L., Salvador, P. A., Rohrer, G. S., *Nanoscale* **2014**, *6*, 24. b)Bai, S., Jiang, J., Zhang, Q., Xiong, Y., *Chem. Soc. Rev.* **2015**, *44*, 2893. c)Yu, J., Wang, W., Cheng, B., Su, B.-L., *J. Phys. Chem. C* **2009**, *113*, 6743.
[26] Liu, J., Liu, Y., Liu, N., Han, Y., Zhang, X., Huang, H., Lifshitz, Y., Lee, S.-T., Zhong, J., Kang, Z., *Science* **2015**, *347*, 970.
[27] a)Ran, J., Ma, T. Y., Gao, G., Du, X.-W., Qiao, S. Z., *Energy Environ. Sci.* **2015**, *8*, 3708. b)Vinu, A., Srinivasu, P., Sawant, D. P., Mori, T., Ariga, K., Chang, J.-S., Jhung, S.-H., Balasubramanian, V. V., Hwang, Y. K., *Chem. Mater.* **2007**, *19*, 4367.

[28] a) Wu, Q., Xu, J., Yang, X., Lu, F., He, S., Yang, J., Fan, H. J., Wu, M., *Adv. Energy Mater.* **2015**, *5*, 1401756. b) Primc, D., Zeng, G., Leute, R., Walter, M., Mayrhofer, L., Niederberger, M., *Chem. Mater.* **2016**, *28*, 4223.

[29] Zhang, J., Yu, J., Zhang, Y., Li, Q., Gong, J. R., *Nano Lett.* **2011**, *11*, 4774.

[30] a) Froschl, T., Hormann, U., Kubiak, P., Kucerova, G., Pfanzelt, M., Weiss, C. K., Behm, R. J., Husing, N., Kaiser, U., Landfester, K., Wohlfahrt-Mehrens, M., *Chem. Soc. Rev.* **2012**, *41*, 5313. b) Hossain, M. K., Koirala, A. R., Akhtar, U. S., Song, M. K., Yoon, K. B., *Chem. Mater.* **2015**, *27*, 6550.

[31] a) Liang, Q., Li, Z., Huang, Z. H., Kang, F., Yang, Q. H., *Adv. Funct. Mater.* **2015**, *25*, 6885. b) Weller, T., Sann, J., Marschall, R., *Adv. Energy Mater.* **2016**, *6*, 1600208.

[32] a) Nath, R. K., Zain, M. F. M., Jamil, M., *Renewable Sustainable Energy Rev.* **2016**, *62*, 1184. b) Magesh, G., Kim, E. S., Kang, H. J., Banu, M., Kim, J. Y., Kim, J. H., Lee, J. S., *J. Mater. Chem. A* **2014**, *2*, 2044. c) Shibata, H., Ogura, Y., Sawa, Y., Kono, Y., *Biosci. Biotechnol. and Biochem.* **1998**, *62*, 2306.